JOURNAL OF PROPULSION AND POWER
Vol. 12, No. 1, January–February 1996

Anode Heat Loss and Current Distributions in a DC Arcjet

Kazuhisa Fujita* and Yoshihiro Arakawa†
University of Tokyo, Tokyo 113, Japan

An experimental and analytical investigation of a low-power DC arcjet was undertaken for the purpose of understanding the arc-column behavior and electrode heat-loss characteristics. Diagnostic measurements were conducted by using an arcjet with axially split anodes with argon as the propellant. Experimental results show that the ratio of electrode gap to constrictor diameter, total current, and chamber pressure have strong effects on the current distribution. Anode heat loss is chiefly transferred by electron flux and thermal conduction of the gas, both of which are closely related to the current distribution. When the current is distributed to the upstream part of the constrictor, the anode heat loss is mostly due to thermal conduction in the downstream part of the constrictor. On the other hand, as the current becomes distributed downstream, the anode heat loss can be reduced due to a cold-gas envelope formed around the arc column in the constrictor. Two-dimensional analysis reveals that the cold-gas envelope becomes heated and decreases in thickness gradually along with streamwise position due to thermal conduction from the arc, while the arc column increases in diameter and finally attaches to the anode wall.

Nomenclature

E = electric field vector
h_0 = total enthalpy of propellant before heating
I = total current
I_d = current distributed to downstream anode
j = current density vector
$\dot{m}$ = propellant mass flow rate
Q_a = anode heat flux
q = heat flux vector
R_g = ratio of electrode gap to constrictor diameter
T = temperature
V = discharge voltage
η_a = anode heat loss fraction
κ = thermal conductivity

Introduction

THE DC arcjet is one of the most promising electric propulsion devices for long-term space missions. Recently, interest in DC arcjets has renewed[1,2] due to the impending availability of several killowatts of electric power onboard spacecraft. However, DC arcjets can often be operated in the low-voltage mode, which is characterized by poor thruster performance and frequent electrode damages.[3,4] It is important to avoid such an undesirable discharge mode in which the arc attaches to the upstream edge of the constrictor. The transition from the low- to high-voltage mode operation may be dependent on the electrode geometry, propellant mass flow rate, and power level. It follows that mechanisms that dominate the arc discharge and propellant flow should be better understood in order to give design guidelines for performance enhancement from a theoretical standpoint.

The heat transfer from the arc column is an important process because it largely influences thermal efficiency, discharge mode, operational stability, and thrust efficiency of DC arcjets. Previous studies of a DC arcjet with water-cooled segmented anodes[5] and two-dimensional analyses[6] have shown that the anode heat loss is closely related to the discharge current distribution. Also, it has been found that the thermal conduction of the gas and the electron flux absorbed by the anode wall are mainly responsible for electrode heating. The thermal conduction of the gas is subject to the temperature distribution in the constrictor, i.e., the thermal constriction of the arc column, and the electron flux is associated with the total discharge current. Numerical results have predicted that the thruster performance is determined by the discharge conditions in the constrictor, where a slight change in propellant heating can drastically influence the flow characteristics. Therefore, an anode split at the constrictor is newly utilized in the present study in order to examine detailed characteristics of the arc-column behavior and heat transfer mechanisms in the constrictor.

Experimental Apparatus

A schematic diagram of the DC arcjet used in the experiment is shown in Fig. 1. The electrode configuration is shown in Fig. 2. The cathode, which is made of 2% thoriated tungsten, is an 8-mm-diam cylindrical rod with a conical tip. The electrode gap, which is defined in Fig. 2, is adjustable by moving the cathode section. The anode is split into an upstream and a downstream segment, as illustrated in Fig. 2. Both the segments are made of tungsten covered with copper water jackets and are thermally and electrically insulated from each other by an insulator disk and gaskets between them.

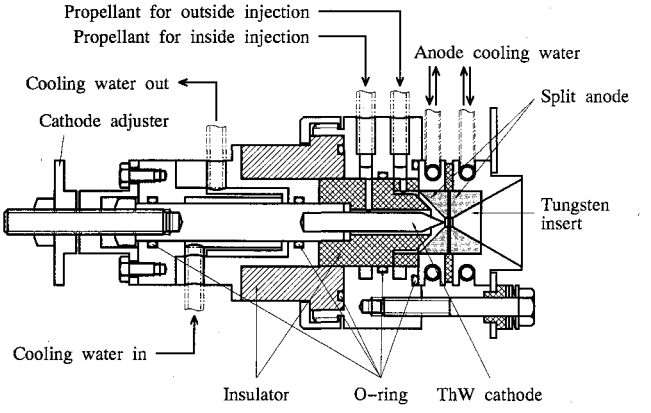

Fig. 1 Schematic cross section of DC arcjet.

Received Dec. 17, 1993; revision received March 27, 1995; accepted for publication April 4, 1995.

*Graduate Student, Department of Aeronautics and Astronautics, 7-3-1, Hongo, Bunkyo-ku.

†Professor, Department of Aeronautics and Astronautics, 7-3-1, Hongo, Bunkyo-ku. Senior Member AIAA.

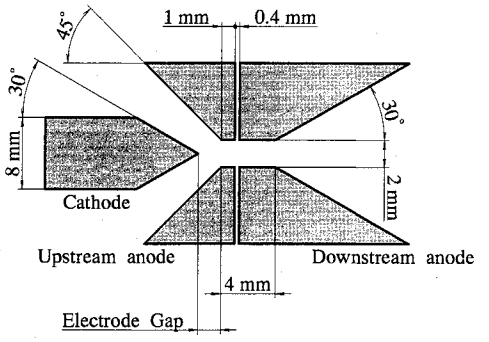

Fig. 2 Electrode configuration.

This allows for measuring the heat flux and discharge current distributed between the anode segments.

The experiment was performed in a 0.5-m-diam- and 2-m-long-vacuum tank of stainless steel, evacuated by a mechanical booster, backed up by three rotary pumps. The background pressure in the tank was maintained below 10 Pa during operation. The propellant was fed to the arcjet through thermal mass flow controllers. A dc power supply incorporates a three-phase full wave selenium rectifier and a saturated reactor controller with an open-circuit voltage of 90 V. The arc discharge was initiated by applying an rf voltage of 4 kV. The discharge current and voltage were measured by series and shunt resistors of 0.6 mΩ and 10 kΩ, respectively. The pressure in the plenum chamber was measured by a diaphragm manometer. In order to obtain the heat flux distribution, all electrodes were separately water-cooled with independent water lines. The heat flux was evaluated from the water mass flow rate and temperature rise, which were measured by a flow meter and chromel–alumel thermocouples, respectively. It normally took several minutes for the arcjet and measurement system to establish thermal equilibrium, after which all of the measurements were performed.

Experimental Results

In the present study, argon was employed as the working gas because it is stable in electrical and thermochemical behavior. It is easy to observe the motion of the arc attachment in the constrictor from the upstream to downstream anode segment because the arc can be attached to the close vicinity of the split between the anode segments. The use of argon may have limited practical relevance to flight arcjets, however, we can obtain general trends of the arc-column behavior and heat-loss characteristics along with the electrode gap, propellant mass flow rate, and current level. The propellant mass flow rate was changed from 89 to 417 mg/s. The operation was performed with variation in current from 50 to 120 A. R_g was introduced to quantitatively examine geometrical effects on the arc-column behavior in the constrictor. The value of R_g was adjusted from 0 to 2.0 in the experiment, which corresponds to the change in electrode gap from 0 to 4.0 mm.

Current Distributions

Figures 3 and 4 illustrate the current distribution characteristics plotted in terms of I_d/I as a function of the plenum chamber pressure. Generally, an increase in pressure increases I_d/I, which implies an increase in arc-column length. It is because a larger amount of propellant requires longer contact with the arc column to be sufficiently ionized to let the current be driven through the propellant gas. On the other hand, I_d/I decreases as R_g increases. This suggests that the arc attachment moves on the constrictor surface in conjunction with the cathode movement if the chamber pressure and current are kept constant. Figure 4 shows that with $R_g = 0.0$, I_d/I increases more quickly along with the pressure, and decreases more with an increase in current than it does with $R_g = 0.5$. This implies that the arc attachment is located in close vicinity of the split between the upstream and downstream segments when $R_g = 0.0$ and that the arc column length increases with increasing the pressure and decreasing the current. However, as the current is distributed upstream with increasing R_g, the current distribution becomes less dependent on the pressure and current, because the arc attachment only moves on the surface of the upstream anode.

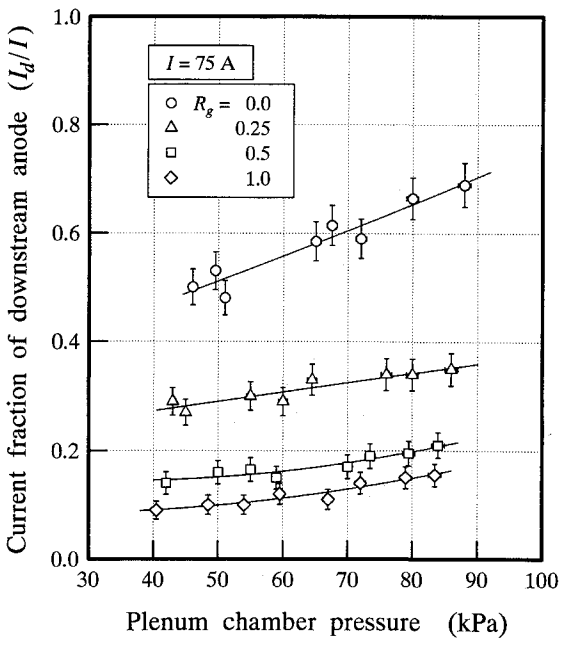

Fig. 3 Current fraction of downstream anode vs plenum chamber pressure for various R_g.

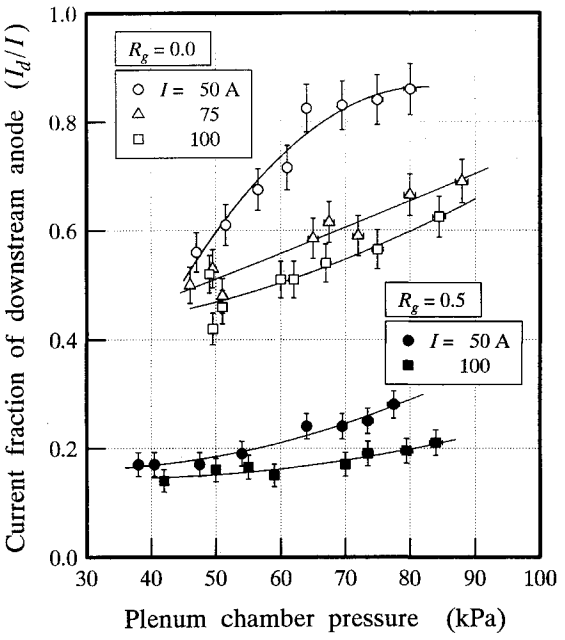

Fig. 4 Current fraction of downstream anode vs plenum chamber pressure for various currents.

Thermal Characteristics

The heat flux to the cathode is small compared with that to the anode. The major portion of the electrode heat loss is deposited in the anode. The cathode heat flux is slightly dependent on the current distribution; however, it remains be-

low 6% of the electric input power, and 10% of the total electrode heat loss. Here, η_a is defined by

$$\eta_a = Q_a/(\dot{m}h_0 + IV) \quad (1)$$

where h_0 is estimated from the plenum chamber pressure and the inlet gas temperature.

Figure 5 is a typical example of η_a plotted against the current for two different mass flow rates, 89 and 387 mg/s. The effects of changes in electrode gap are also shown in terms of R_g. An increase in mass flow rate decreases η_a and an increase in current increases η_a. This suggests that a large amount of propellant suppresses the heat conduction and thermally isolates the anode surface from the arc column. On the other hand, the heat transfer from the arc is increased with increasing the current. The increase of η_a along with R_g is due to a change in distributions of the current and gas temperature in the constrictor. With increasing R_g the high-temperature region of the gas is distributed upstream of the constrictor along with the current, and the majority of the constrictor wall downstream from the arc attachment is exposed to the high-temperature gas, which increases the heat conduction to the anode surface.

The variation of the upstream and downstream portions of η_a is shown in Fig. 6 as a function of the plenum chamber pressure. The current fraction of the downstream anode is also presented in order to show a relation between them. An increase in pressure is found to have the multiple benefits of thermally isolating the upstream anode from the high temperatures and distributing the current to the downstream anode, both of which remarkably decrease the heat flux to the upstream anode. The heat loss fraction of the downstream anode increases along with the current fraction of this segment because of an increase in electron flux, although it seems to saturate, even decrease, at chamber pressures higher than 70 kPa. This suggests that the electron flux is chiefly responsible for the heat loss transferred to this segment, while the thermal conduction is also suppressed due to the constriction of the arc column. A reduction of the total anode heat loss fraction is associated with a decrease in thermal conductive transfer from the arc column in the upstream region of the constrictor.

To investigate how the conduction loss can be reduced in the upstream portion of the constrictor, the upstream anode is switched off and electrically floated. Hence, the current is redistributed to the downstream anode only, and the heat flux to the upstream anode is mainly transferred by thermal conduction and radiation, although the latter is of little significance in comparison with the former.[5] A typical result with I = 100 A and R_g = 1.0 is shown in Fig. 7. It is found that the upstream portion of the heat-loss fraction largely decreases with increasing the chamber pressure, while the downstream portion is less dependent on the pressure. This leads to an important conclusion that the thermal conduction mainly causes the heat loss to the upstream anode, which can be largely reduced by constricting the arc. In addition, the heat loss is chiefly transferred to the downstream anode by the electron flux, which is independent of the pressure, but dominated by the number of electrons, namely, the discharge current. A slight decrease in heat loss to the downstream anode with increasing the pressure is also due to a decrease

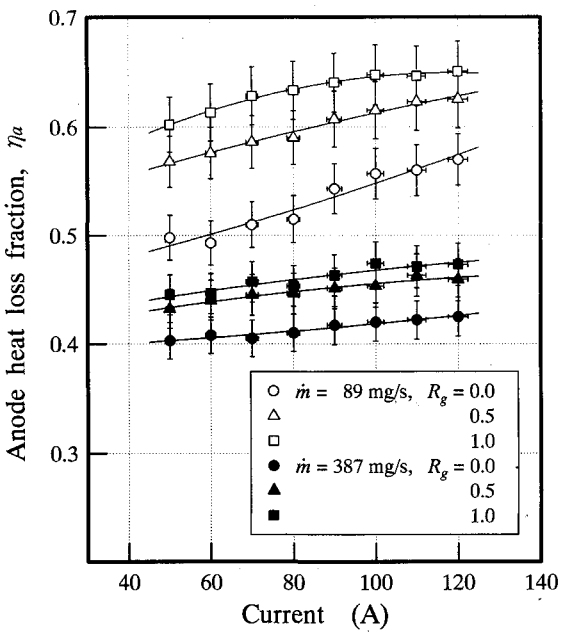

Fig. 5 Characteristics of anode heat loss fraction for various R_g.

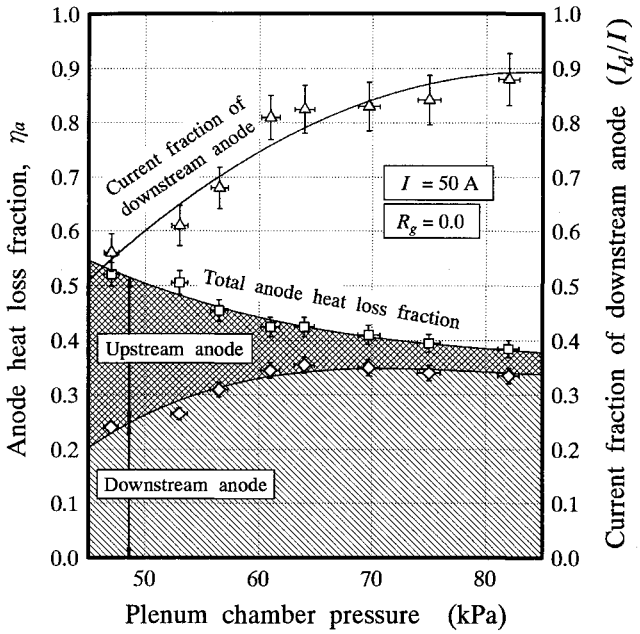

Fig. 6 Variations of current and anode heat loss fractions as a function of plenum chamber pressure.

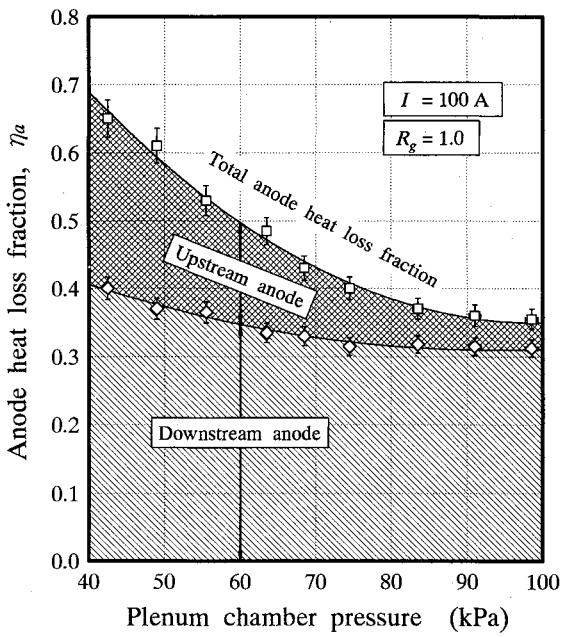

Fig. 7 Variation of anode heat loss fraction with switching off and electrically floating upstream anode.

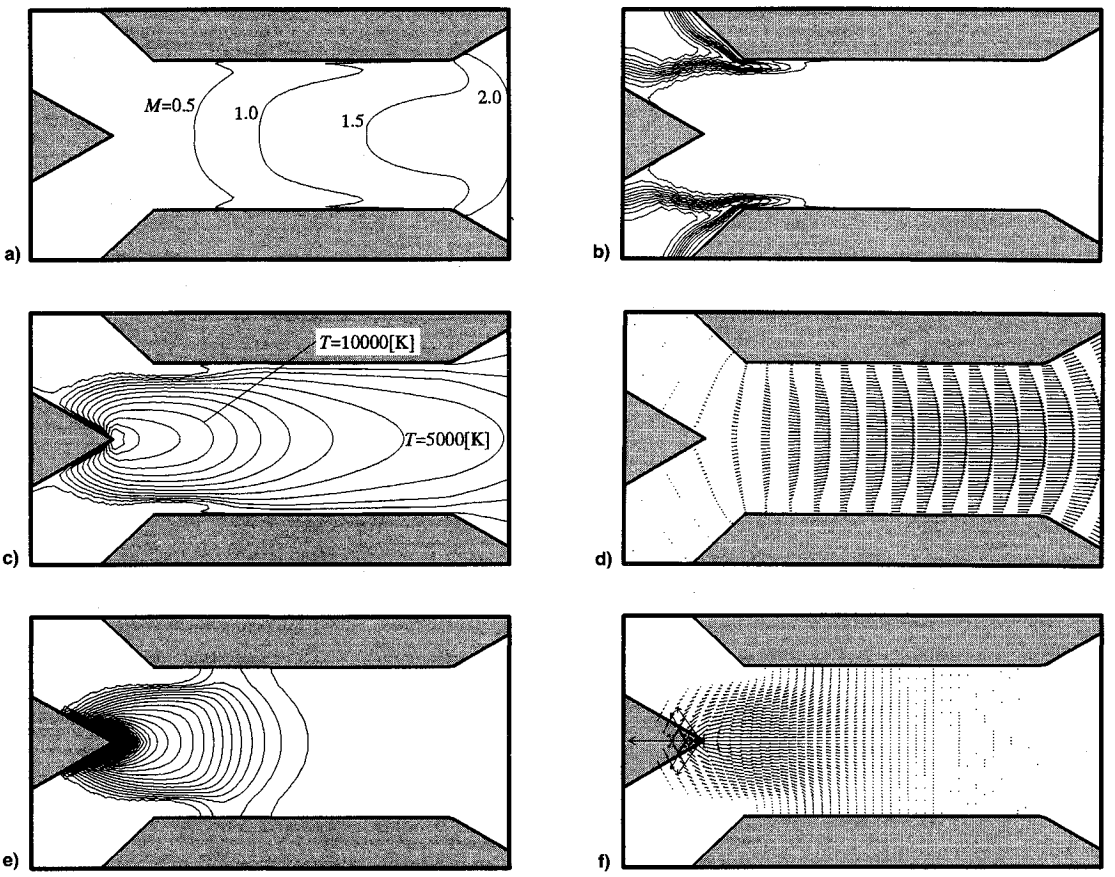

Fig. 8 Example of calculated distributions of a) Mach number, b) mass density, c) temperature, d) velocity vectors, e) current density, and f) current density vectors ($\dot{m}$ = 208 mg/s, I = 80 A, R_g = 0.25; magnified detail drawings of constrictor region).

in conduction loss, which is brought about by a decrease in gas temperature.

Two-Dimensional Numerical Analysis

Numerical Model

A two-dimensional numerical analysis was performed for the arcjet used in the experiment in order to obtain qualitative understandings of phenomena in the constrictor region. Because of the existence of the arc column at the thruster center axis in the constrictor, thermodynamic and electromagnetic properties of arcjet flow change drastically according to position in the axial and radial direction. Therefore, for the purpose of this study, a simple but two-dimensional model is used rather than multichannel models in a quasi-one-dimensional manner[7] or performance-predictable codes[8,9] in more sophisticated approaches with high complexity.

Argon is assumed to be partially ionized plasma composed of electrons, singly charged ions, and neutral atoms. The flow is assumed to be laminar and inviscid, although the mean Reynolds number is estimated to be 10^3 in the constrictor. Radiative heat transfer can be ignored in comparison with thermal conduction.[8] The Lorentz force due to the self-induced magnetic field is neglected because of the small current involved. The flow and the electric field are assumed to be axisymmetric and azimuthal components are neglected. In addition, the local thermal equilibrium is assumed to be established, and all of the transport properties are evaluated based on the equilibrium conditions, except at both ends of the arc column where the electrode potential drop exists.

The unsteady Euler equations in the cylindrical system, including heat conduction ($\boldsymbol{q} = -\kappa\nabla T$) and Joule heating ($\boldsymbol{j}\cdot\boldsymbol{E}$) in the energy equation, are transformed using the rectangular curvilinear coordinates numerically obtained for the arcjet flow channel. The transformed equations are numerically solved by the Harten–Yee explicit symmetric total variation diminishing scheme[10,11] to obtain steady-state solutions. On the other hand, a steady-state elliptic equation of the electric potential is introduced by excluding effects of the magnetic field from the Maxwell's equations and Ohm's law. It is solved by the finite element method in each iteration of the flow calculation, making use of the same rectangular grid system. Further detailed descriptions of the arcjet model and numerical procedures are given in Ref. 12.

Results and Discussion

Numerical simulations were performed for two propellant mass flow rates, 89 and 208 mg/s, with a variation of discharge current from 60 to 120 A and R_g from 0 to 0.5. All of the computations were done on a HP 9000/730 computer. Because of the strong nonlinearity of heat generation and thermal conduction in the source term, the Courant–Friedrichs–Lewy number was limited below 0.075 for computational stability. A steady state is obtained after the first 3×10^5 time steps from initiation, which takes about 8 h in a single simulation.

As a typical example of a calculation result, Fig. 8 shows magnified detail drawings of the constrictor region. From the Mach number contours, it is found that the flow turns supersonic just after the point of anode attachment. The arc column is located at the thruster axis, surrounded by a cold-gas envelope with low temperature and high mass density. Due to the thermal conduction from the arc, the cold-gas envelope gradually shrinks while the arc column increases in diameter, and finally, the arc attaches to the anode, ending the cold-gas envelope.

The anode heat loss fraction is also evaluated by Eq. (1) in the simulation. The variation of calculated η_a is plotted against the current in Fig. 9. The numerically obtained η_a shows qualitative agreement with the thermal conductive

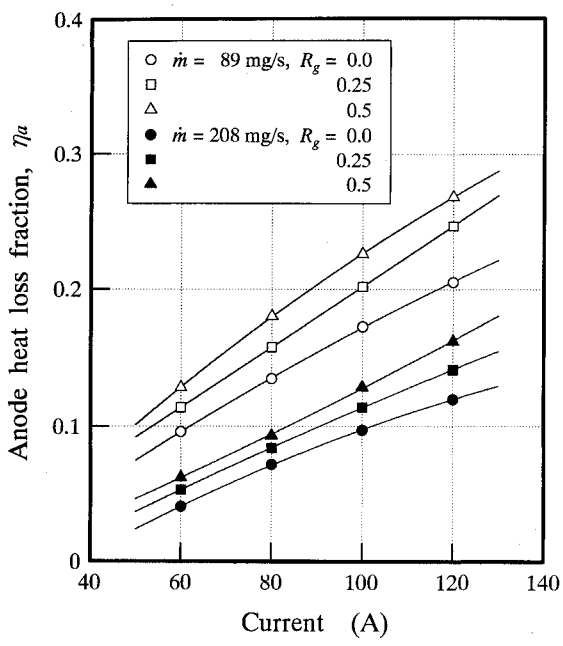

Fig. 9 Characteristics of numerically obtained anode heat loss fraction.

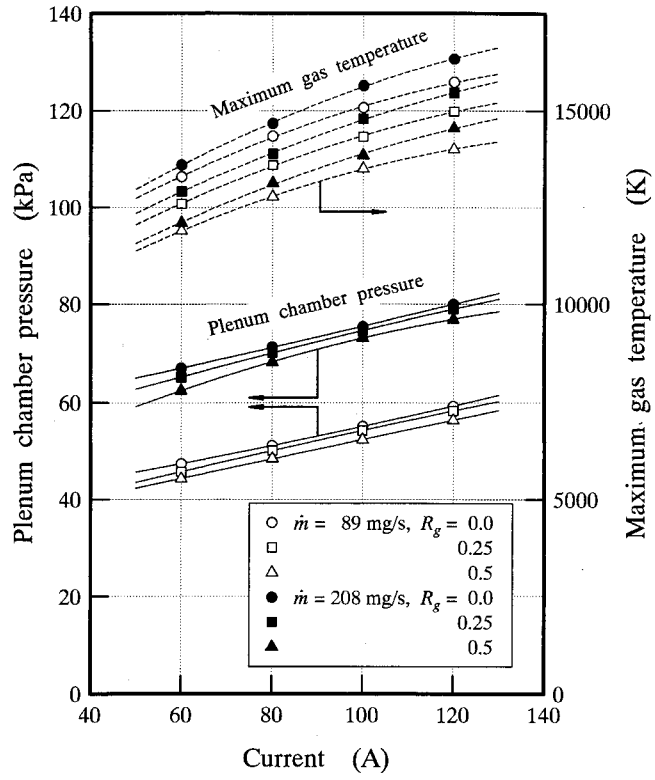

Fig. 10 Calculated maximum gas temperatures and plenum chamber pressures.

characteristics derived from the experimental results, namely, an increase along with the current and R_g and a decrease with increasing the mass flow rate. However, because neither the radiative heat transfer nor electron flux absorption in the electrode surface is taken into account, the anode heat flux is only caused by the thermal conduction of the gas and values of calculated η_a are smaller than the experimental ones. Also, the line slopes of η_a are rather different, indicating that the model overpredicts the effect of current on η_a. It is because the arc attachment is calculated to move more quickly in the downstream direction than observed in the experiment with decreasing the current. This leads to the smaller portion of the constrictor wall exposed to the high-temperature gas, underestimating the anode heat loss fraction.

In the calculated flowfield, the gas temperature is found to be the highest just downstream of the cathode tip. The maximum gas temperature for each mass flow rate and R_g is shown in Fig. 10. The calculated plenum chamber pressures are also plotted in this figure. The numerical prediction of pressure is found to agree with the experiment, although the measured values are not compared in this figure. It is noted that when the propellant mass flow rate is increased, the maximum gas temperature does not decrease, but slightly increases. This fact suggests that an increase in mass flow rate does not uniformly decrease the gas temperature in the whole flowfield, but changes its distribution to a sharper radial profile in such a way to decrease the temperature of the cold-gas envelope and to increase the plasma temperature at the center. A larger amount of propellant passes through the region with high pressure and density around the arc column, which confines and constricts the high-temperature arc column at the center. It is also found that the maximum gas temperature decreases with increasing R_g in Fig. 10, accompanied by a larger anode heat loss fraction as seen in Fig. 9. This is because the constriction of the arc column is somewhat relaxed. When the arc column is located in the constrictor, the thermal energy transferred from the arc into the surrounding cold-gas envelope is immediately carried downstream due to the high speed of the stream. Conversely, when the arc column is located upstream of the constrictor where the flow is at relatively low speeds, its diameter increases rapidly along with streamwise position, and the high-temperature plasma is not well confined.

In Figs. 11a–11d, distributions of the temperature, current density, current to the anode, and the anode heat flux for four different operation points are compared. The arcjet is operated with $\dot{m}$ = 89 mg/s, I = 100 A, and R_g = 0.5 in Fig. 11a. Here, the arc column is found widespread in the plenum chamber and the anode heat flux is significantly transferred from the arc. A decrease of R_g in Fig. 11b confines the high-temperature gas at the center, redistributes both the current and anode heat flux to the downstream part of the constrictor, and reduces the anode heat flux in comparison with Fig. 11a. In Fig. 11c, the propellant mass flow rate is raised to 208 mg/s, which redistributes the current and anode heat flux more downstream and constricts the arc column in comparison with Fig. 11b. With a large amount of propellant given for a relatively small current, the arc column is more intensely constricted, as seen in Fig. 11d. In this case, a large area of the constrictor wall is insulated from the arc, and only the small portion downstream from the arc attachment is in contact with the high-temperature gas, which can eventually decrease the anode heat loss.

As discussed previously, an increase in plenum chamber pressure has the multiple benefits of constricting the arc column, increasing the arc column length, increasing the discharge voltage, and correspondingly decreasing the current in case of constant electric input power. The constriction of the arc column confines the high-temperature gas at the center axis by corresponding development of the cold-gas envelope around the arc column, and a decrease in current reduces the electron flux absorbed in the anode, both of which will contribute to high thermal efficiencies of DC arcjets. From a thruster design standpoint, a decrease in constrictor diameter is considered to be effective because it can raise the plenum chamber pressure without excessively increasing the propellant mass flow rate and decreasing the gas enthalpy. This numerical model should undergo further improvement to precisely predict the practical phenomena and even the thruster performance.

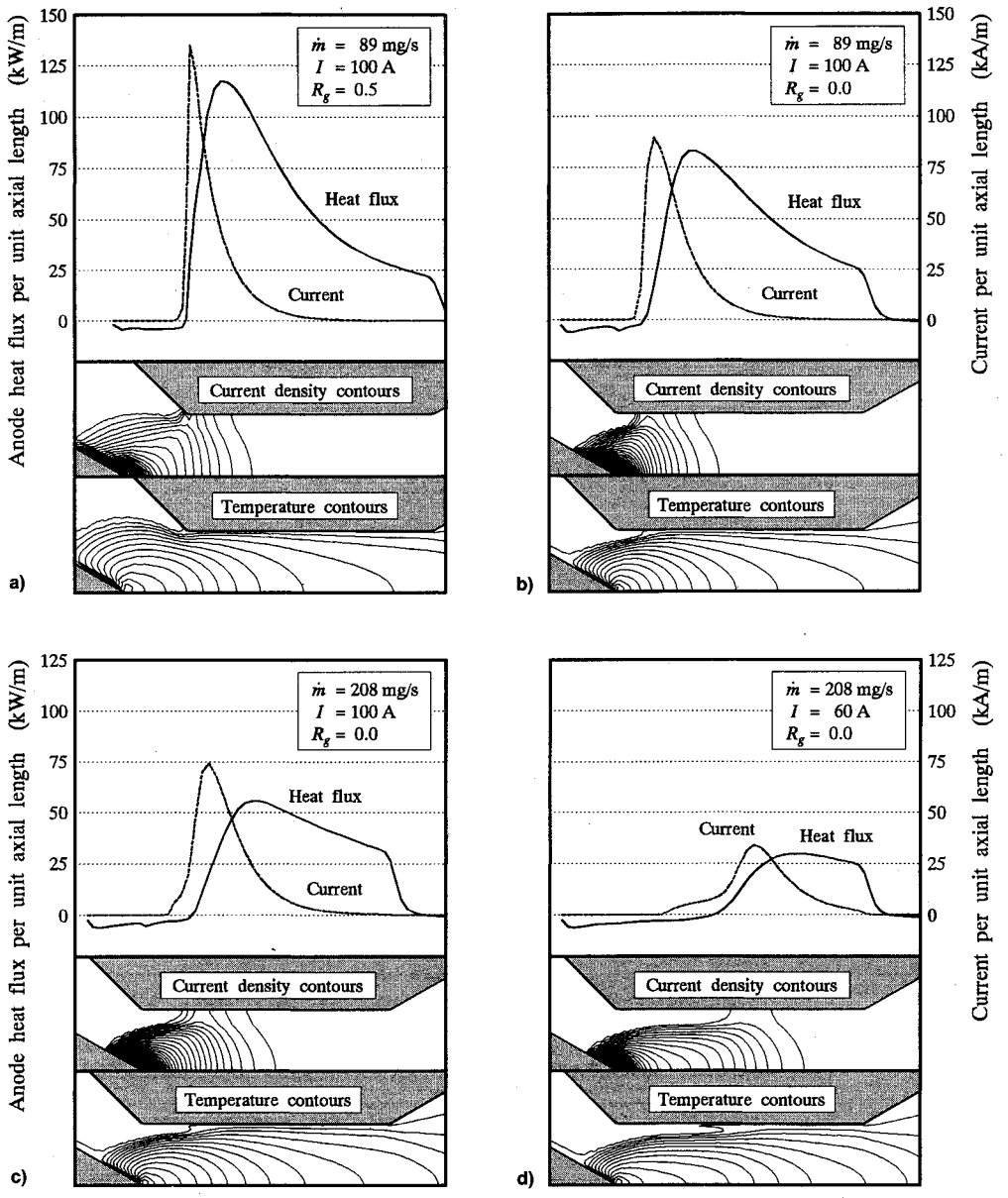

Fig. 11 Distributions of anode heat flux and current along the constrictor wall in comparison with current and temperature contours in flowfield: a) $\dot{m}$ = 89 mg/s, I = 100 A, R_g = 0.5; b) $\dot{m}$ = 89 mg/s, I = 100 A, R_g = 0.0; c) $\dot{m}$ = 208 mg/s, I = 100 A, R_g = 0.0; and d) $\dot{m}$ = 208 mg/s, I = 60 A, R_g = 0.0; contours are drawn at the same intervals.

Summary

Experimental results show that the discharge current distribution depends on the total discharge current, the plenum chamber pressure, and the electrode geometry. The thermal energy deposited in the anode surface is chiefly transferred by electron flux absorbed by the anode and by thermal conduction of the gas. The electron flux is related to the total discharge current, whereas the thermal conduction is strongly dependent on the development of the cold-gas envelope around the arc column. The anode heat loss decreases with the arc attachment entering the constrictor and being located downstream because the cold-gas envelope is formed around the arc column. This confines the arc at the center and thermally and electrically insulates a large portion of the constrictor surface from the high-temperature plasma core.

A two-dimensional numerical analysis agrees well with the experimental results and explains the arc-column behavior in detail. In contact with the arc column, the cold-gas envelope becomes heated and decreases in thickness gradually along with streamwise position due to thermal conduction from the arc column. The arc column conversely increases in diameter and finally expands to attach to the anode wall.

References

[1]Sankovic, J. M., Hamley, J. A., Haag, T. W., Sarmiento, C. J., and Curran, F. M., "Hydrogen Arcjet Technology," 22nd International Electric Propulsion Conf., IEPC-91-018, Viareggio, Italy, Oct. 1991.

[2]Smith, W. W., and Cassady, J. R., "Arcjet Technology Improvement," Rocket Research Co., 86-R-1063, AFRPL-TR-86-079, Dec. 1986.

[3]Ishii, M., and Kuriki K., "Optical and Analytical Studies of Arc Column in DC Arcjet," AIAA Paper 87-1086, May 1987.

[4]Glocker, B., Auweter-Kurtz, M., Goelz, T. T., Kurtz, H. L., and Schrade, H. O., "Medium Power Arcjet Thruster Experiments," AIAA Paper 90-2531, July 1990.

[5]Fujita, K., and Arakawa, Y., "Heat Loss and Current Distributions in a DC Arcjet Thruster," *Journal of the Faculty of Engineering, The University of Tokyo*, Vol. XLII, No. 1, 1993, pp. 15–39.

[6]Fujita, K., "Heat Loss and Acceleration Mechanisms of a Low Power DC Arcjet," *Proceedings of the 18th International Symposium*

on Space Technology and Science (Kagoshima, Japan), May 1993, pp. 2529–2534.

[7]Schrade, H. O., and Sleziona, P. C., "Performance Calculation of an H_2 Arcjet by Means of a Dual Channel Model," AIAA Paper 88-104, Oct. 1988.

[8]Miller, S., and Martinez-Sanchez, M., "Nonequilibrium Numerical Simulation of Radiation-Cooled Arcjet Thrusters," 23rd International Electric Propulsion Conf., IEPC-93-218, Seattle, WA, Sept. 1993.

[9]Butler, G. W., Kull, A. E., and King, D. Q., "Numerical Simulations of Hydrogen Arcjet Performance," 23rd International Electric Propulsion Conf., IEPC-93-249, Seattle, WA, Sept. 1993.

[10]Yee, H. C., Warming, R. F., and Harten, A., "Implicit Total Variation Diminishing (TVD) Schemes for Steady-State Calculations," *Journal of Computational Physics*, Vol. 57, No. 3, 1985, pp. 327–360.

[11]Yee, H. C., "Construction of Explicit and Implicit Symmetric TVD Schemes and Their Applications," *Journal of Computational Physics*, Vol. 68, No. 1, 1987, pp. 151–179.

[12]Fujita, K., and Arakawa Y., "Anode Heat Loss and Current Distributions in DC Arcjets," 23rd International Electric Propulsion Conf., IEPC-93-185, Seattle, WA, Sept. 1993.